Using an injection locked VCSEL to produce Fourier Transform-limited optical pulses

JED ROWLAND[1], CHRISTOPHER PERRELLA[1*], PHILIP LIGHT[1], BEN M. SPARKES[1], AND ANDRE N. LUITEN[1]

[*] Corresponding author: chris.perrella@adelaide.edu.au
[1] Institute for Photonics and Advanced Sensing (IPAS) and School of Physical Sciences, University of Adelaide, 5005, SA, Australia

Compiled August 9, 2021

We create Fourier transform-limited, nanosecond scale optical pulses from a vertical cavity surface emitting laser (VCSEL) using injection locking with a narrow-band seed laser. We examine two different injection locking architectures and show that we can achieve an effective injection locking range of over 8 GHz with an extinction ratio of 20,000:1. These results indicate that injection locked VCSELs could become a key component of large-scale photonic quantum networks.

http://dx.doi.org/10.1364/ao.XX.XXXXXX

Pulsed light on the nanosecond to femtosecond time scales has applications across a range of fields from ultrafast optics [1] and classical telecommunications [2] through to quantum communications [3] and computing [4]. In particular, the high bandwidths attainable through photonic quantum networks processing is already motivating the development of GHz-bandwidth quantum memories [5–8], which would allow for increased transmission rates across the network [9], significant improvements in the creation rates of multi-photon quantum states [10], and reducing the resources required to perform two-photon gates [11]. These quantum memories require strong atom-light interactions to operate efficiently, placing restrictions on the bandwidth of the input pulses, which would ideally be Fourier transform-limited [12]. The pulses should also have a high extinction ratio, i.e., ratio of peak power to average power between pulses, and, if it is to be used in a network with many nodes, allow for easy duplication.

Sub-nanosecond, bandwidth-limited optical pulses can be produced directly from lasers via a variety of methods including Q-switching [13], mode-locking [14] and pulsed pumping [15]. However, these systems can be complex with limited operational modes, e.g., fixed repetition rates and pulse durations. More importantly, this approach does not guarantee that the pulses will be Fourier transform-limited. Another option to generate pulsed light is to chop the output of continuous-wave (CW) lasers. Commercially available electro-optic devices such as Mach-Zehnder interferometers (MZI) and Pockels cells can produce variable length bandwidth-limited pulses down to femtosecond durations when driven by fast electronic pulses. However, each of these devices comes with drawbacks. Pockels cells can achieve extinction ratios up to 1,000:1 but require voltage slew rates of kV/ns to produce nanosecond pulses and thus can produce significant electrical noise. MZIs can achieve extinction ratios up to 10,000:1 but typically require strict environmental control, or additional feedback to maintain this, and can have large insertion losses. These drawbacks make them non-ideal when considering scalability to large information processing networks.

Another option is to use a Vertical Cavity Surface Emitting Laser (VCSEL), which can produce picosecond pulses of light with small threshold currents and relatively simple electronics. VCSELs have been used for decades in the telecommunications industry as transmitters of digital information [16] and can be modulated to encode information in the phase, frequency or amplitude of their output. Due to carrier density effects [17], however, their free-running output pulses are subject to large frequency chirps on the scale of GHz to 100s of GHz [18], making them unsuited to many applications, e.g., coupling light to relatively-narrow atomic transitions as required in quantum memories or in coherent communications transmitters [19].

The use of injection locking to restrain frequency chirp is a well-established technique [20] utilized for the power modulation of VCSELs for digital information processing [21]. In this experiment we inject a frequency stable CW laser into an electrically pulsed VCSEL. Two critical properties that measure the quality of an injection locking arrangement are the frequency locking range and the extinction ratio. The locking range, $\Delta\nu_{LR}$, is the total frequency tuning range of the slave while it remains phase coherent with the master laser frequency. The locking range has the general form:

$$\Delta\nu_{LR} = A\sqrt{\frac{P_m}{P_s}}, \tag{1}$$

where P_m and P_s are the optical powers of the master and slave lasers respectively and the constant A has absorbed a number of parameters, e.g., the linewidth enhancement factor and mode coupling coefficient [22]. We define the extinction ratio as the ratio of the peak pulse height of the slave to the reflected master power P_r. Assuming the slave pulse power is constant, then the extinction ratio takes the following form:

$$ER = \frac{P_s}{P_r}. \tag{2}$$

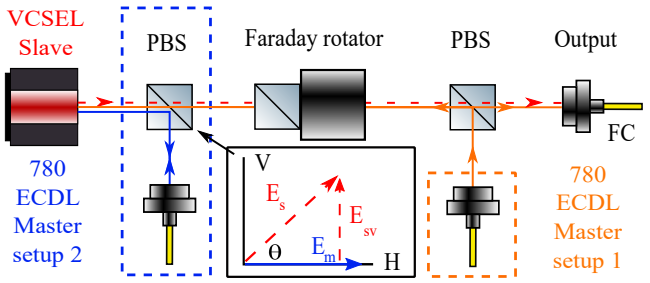

Fig. 1. Injection lock setup consisting of PBS - polarizing beam splitter, VCSEL - vertical cavity surface emitting laser, ECDL - external cavity diode laser, FC - output fibre coupler. The section outlined in orange (blue) is only present for Setup 1 (2). Inset: diagram showing the vertical and horizontal axis for the PBS and the electric field vector for the master E_m, the slave E_s at an angle θ from the PBS horizontal axis, and the vertical component of the slave E_{sv} for Setup 2.

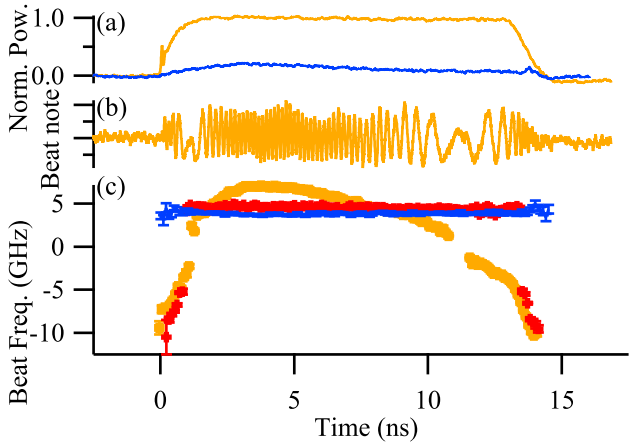

Fig. 2. (a) 13.5 ns pulse power profiles for Setup 1 injection locked (orange) and Setup 2 injection locked (blue), normalized to the max. pulse power for Setup 1. (b) Example of a beatnote of a free-running pulse from the Setup 1. (c) Average instantaneous frequency of Setup 1 free-running (orange) and injection locked (red) and Setup 2 injection locked (blue).

In this paper we investigate two different injection locking architectures: a conventional injection locking setup, and a modified setup that leads to a significant increase in the extinction ratio. We show that in both cases the output pulses are Fourier transform-limited. This is shown by two methods: measurement of the instantaneous frequency of the pulse, and through the spectral properties of the pulse interaction with a narrow two-photon atomic transition. By demonstrating transform-limited pulses along with a high extinction ratio we show that this simple setup is suitable for integration with high-bandwidth quantum memories, thereby opening the door to their use in optical quantum information networks.

The experimental setup consisted of three sections: injection locking, heterodyne measurement, and atom-light interaction.

The master laser was an external cavity diode laser (ECDL) that was tuned to the rubidium (Rb) D2 transition (780 nm). It had a linewidth of less than 1 MHz and was capable of mode-hop free scanning over 8 GHz.

The slave laser was a ULM Photonics 780 nm single mode VCSEL TO46 with maximum power output of 300 μW under continuous operation. A Stanford Research Systems Model DG645 digital delay generator drove the VCSEL, producing optical pulses as short as 1.5 ns full width at half maximum (FWHM) with a 0.173 ns timing jitter and 10% peak height root mean square power fluctuation. Its centre frequency was temperature tuned and stabilised to $\approx$ 25 °C using a thermo-electric controller. This VCSEL lased in one of two orthogonal polarization modes, with mode selection dependent on factors such as drive current and temperature. As the drive current and temperature both change during pulsed operation the polarization mode can show polarization bi-stability [23]. The polarization matching between the VCSEL and master light can also influence the VCSEL polarization mode and thus it is optimal to polarization match the two.

We implemented two different injection locking setups, both shown in Fig. 1. The difference between the setups was the method by which the master light was injected. In Setup 1 the master was spatially and polarization matched to the slave through a Faraday rotator. This is typical practice when seeding a single transverse mode and results in a maximum optical gain , i.e., slave power out divided by master power in. This presents a problem, however, as the emitted slave light cannot be separated from master light that directly reflects from the front face of the slave, limiting the extinction ratio of the system.

In Setup 2 the master is not injected using the Faraday rotator but via a polarizing beam splitter (PBS) that is inserted between the slave and the rotator. The master light that reflects from the face of the slave is reflected by the PBS on its second pass. However, in order to avoid polarization bi-stability effects, the slave polarization must be rotated to be close to that of the master. The inset of Fig. 1 illustrates this situation. If the angle (θ) between the slave polarization and the horizontal PBS axis is reduced to better polarization match the slave to the master, less slave power is transmitted back through the PBS and therefore the optical gain of the system is reduced.

To understand the dynamics of the pulsed injection locked system, we observed the instantaneous frequency of the slave pulses using heterodyne detection. The heterodyne detection setup consisted of a separate frequency-stabilized 780 nm reference laser, combined with the slave pulses using a 50:50 fiber splitter. The beat note was detected on a 20 GHz photodiode amplified using 14 GHz bandwidth amplifiers (setting the bandwidth of our system) and measured on a 110 GHz bandwidth Keysight UXR1102A Infiniium UXR-Series Oscilloscope. Typical chirped data is shown in Fig. 2(b).

The average frequency of the free-running slave was positioned to match the master laser frequency through temperature control. The instantaneous frequency was estimated from the beatnote data by measuring the time between zero-crossings for each cycle of the beat note. To build up statistics, 100 pulsed beat notes were acquired with the instantaneous frequencies binned into 0.1 ns time windows and averaged together, resulting in the frequency profiles shown in Figs. 2 and 3. The error bars are the standard error for each time bin.

Figure 2(c) shows a free-running and injection locked slave pulse with 10 μW of master power for Setup 1. The free-running 13.5 ns pulse has a chirp whose instantaneous frequency travels approximately 15 GHz due to a number of dynamical processes that occur during the pulsing of a semiconductor diode laser including changing charge carrier densities and adiabatic processes [17]. The slave pulse was stabilized for approximately 12.5 ns of its 13.5 ns duration, which corresponds to 92% of the

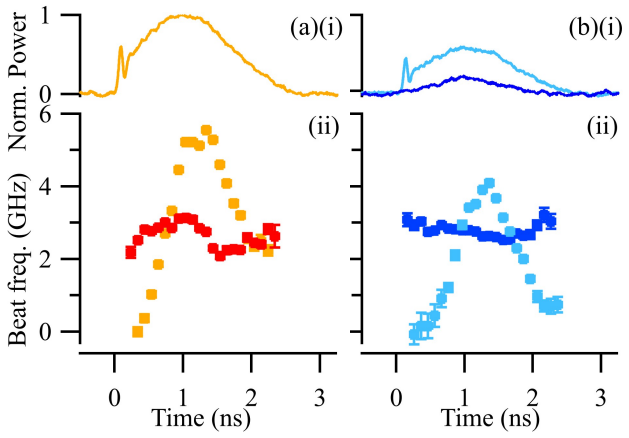

Fig. 3. (a) Setup 1 (i) Free-running normalized 1.5 ns pulse power (identical for injection locked). (ii) Instantaneous frequency for a free-running (orange) and injection locked pulse (red). (b) Setup 2 (i) Pulse power, normalized to the Setup 1 pulse, for a free-running pulse (light blue) and injection locked pulse (dark blue). (ii) Instantaneous frequencies for a free-running pulse (light blue) and injection locked pulse (dark blue).

power in the pulse. In this injection locking arrangement the output power of the slave did not alter from that of the free-running operation.

Fig. 3(a) shows an unlocked and a locked 1.5 ns pulse with 10 μW of master power for Setup 1. The injection locking constrains the instantaneous frequency to a 1 GHz range compared to a 5 GHz range when unlocked. For Setup 2, the two pulses were locked for their full duration. Figs. 2(a) and 3(b)(i) show the power profiles for a 13.5 ns locked pulse (blue) and 1.5 ns unlocked and locked pulses. It can be seen that there are significant differences in power between the two cases due to PBS attenuation.

The extinction ratio was measured after the output fiber coupler as a function of master laser power. As shown in Fig. 4, this shows good agreement with the expected behaviour as a function of master laser power (Eq. 2) for both setups.

The locking range of the slave was estimated by generating pulses of 1.5 ns length with a 6 MHz repetition rate. The master

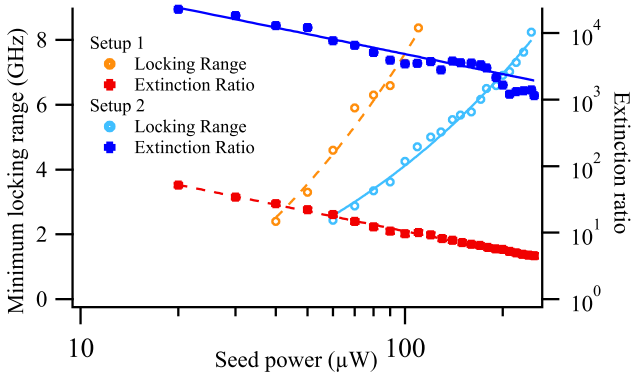

Fig. 4. Minimum locking range and extinction ratio measurements as a function of seed power for both setups. Data is fitted with Eq. 1 or Eq. 2 respectively.

frequency was then scanned across the D2 transition of Rb. The slave pulses were sent through a Rb vapor cell and the corresponding absorption spectrum measured. We observe that the slave transmission spectrum matches the master laser transmission for the spectral range over which it is locked. In order for the slave laser to maintain phase coherence with the master laser when the slave is being pulsed, and the master is being scanned over some range, it is necessary for the injection locking range to be at least as wide as the scan range plus the Fourier width of the pulse. This is assumed to be the maximum locking range. As the dynamics of these two processes are very different we have just adopted the scan range. We term this the minimum locking range. An optical reference cavity with a free spectral range of ≈300 MHz was used to determine a linear frequency scale. The minimum locking range of the slave was investigated as a function of master laser power and, from Fig. 4., it can be seen that the locking range behaves as expected from Eq. 1. The maximum locking range that we could observe using this method is the width of the Rb D2 transition. Increasing the master laser power will continue to increase the locking range, as per Eq. 1, at the cost of a reduced extinction ratio.

A horizontal offset can be seen in the locking range curves in Fig. 4 as roughly 20 μW of seed power is required to stabilize the pulse's instantaneous frequency chirp. The maximum extinction ratio of 100:1 is relatively low due to the seed light reflecting off the VCSEL surface having the same spatial and polarization mode as the slave pulse. The optical gain of the peak slave power compared to the master input power was 2 dB.

The extinction ratio is improved for Setup 2. This results in GHz locking ranges being achieved with extinction ratios up to 20,000:1. There are a number of trade-offs for the significantly improved extinction ratio of Setup 2. The first is loss of slave pulse power at the output, resulting from the polarization being rotated from the transmission axis of the PBS as can be seen in the dark blue trace in Fig. 3 (b)(ii). This resulted in an optical gain of -3 dB. The second trade-off arrises from polarization switching during the pulse, as the laser can switch between the two orthogonal polarization modes within the duration of a single pulse. When combined with polarization filtering such as a PBS, this can result in a deterioration of the output pulse shape. With careful selection of powers and polarisations, however, polarization bistable switching can be avoided, as is shown here.

To efficiently interact pulsed light with narrow-linewidth atomic transitions the light needs to have an appropriately narrow bandwidth [12]. To provide an unambiguous measurement of the individual pulse bandwidth, we used a two-photon atomic absorption scheme within a hollow-core photonic crystal fiber (HCPCF) filled with Rb vapor, which facilitates strong light-atom interactions [24, 25]. The slave pulses were sent through the HCPCF along with a counter-propagating CW 776 nm ECDL laser that together drove the ^{87}Rb $5S_{1/2}\rightarrow 5D_{5/2}$ two-photon transition. The 776 nm laser frequency was stationary while the slave pulse was locked to the 780 nm master laser, which was scanned across a range of several GHz corresponding to the relevant region of the Rb D2 transition. A lock-in amplifier was referenced to the slave's 100 kHz pulse repetition rate, rejecting background master light, while another lock-in was referenced to the 776 nm laser that was switched on and off at 5 kHz using an acousto-optic modulator. This allowed us to extract the relatively small two-photon absorption signal from the background 780 nm transmission. An example of the output from the double lock-in is shown in the inset of Fig. 5.

The four underlying hyperfine absorption components of

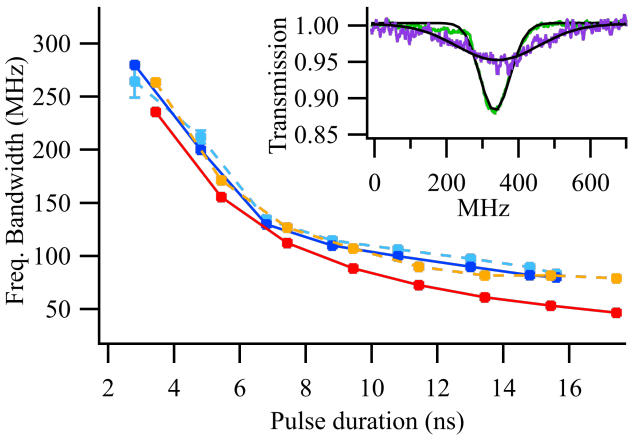

Fig. 5. Frequency FWHM calculated by Fourier analysis and two-photon absorption for Setup 1 (red and orange respectively) and Setup 2 (dark and light blue respectively). Inset: example of two-photon absorption of a 20 ns pulse (green) and a 6 ns pulse (purple) with their respective function fits (black).

the ^{87}Rb $5S_{1/2}\rightarrow 5D_{5/2}$ transition were fitted with Voigt functions. The amplitudes and frequency spacings of the individual components were fixed at known ratios and intervals [26]. The Lorentzian components of the Voigt were kept at a constant width previously determined from transit-time broadening [25]. The Gaussian component includes fixed offsets for both transit-time broadening and residual Doppler-broadening, as well as the spectral width of the pulse. This final component represents the bandwidth of the slave pulses. The results of this analysis for various pulse lengths are shown in Fig. 5.

To determine the performance of the injection lock, the measured bandwidths of the pulses were compared to their transform-limited values derived from Fourier transforms of the pulse profiles. The Fourier transform-limited bandwidths and the measured bandwidths are displayed in Fig. 5. It can be seen that the slave pulses are near or at the Fourier transform limit for all pulse lengths and both setups investigated.

While Setup 2 results in less output power compared to Setup 1, overall, this unconventional setup produces nanosecond pulses with an extinction ratio of over 20,000:1 for a Fourier transform-limited pulse bandwidth of 250 MHz, a wavelength resonant with a strong atomic transition [8], and an optical gain of -3 dB. This places it above or equal in performance to other devices that can generate optical pulses from CW lasers such as Pockels cells or MZIs. This technique is also easily scalable, with a 100 mW master laser able to stabilize 25,000 VCSELs, assuming 50% fiber-coupling losses. Further improvements in scalability are envisaged if the VCSELs were incorporated into a single optical wafer [27]. Such a development would not only allow for an increase in the size of photonic quantum networks, but also for applications in current classical telecommunications networks.

In conclusion, we have shown that it is possible to reduce the frequency chirp of VCSEL-derived nanosecond pulses to the Fourier transform-limit using injection locking. We demonstrated an extinction ratio of over 20,000:1 and reduction of the instantaneous frequency chirp of a 13.5 ns pulse from 15 GHz to ≈10 MHz, and a 1.5 ns pulse reduced from 5 GHz to 0.5 GHz. We confirmed this increased spectral purity by investigating the two-photon interaction of pulses in Rb vapor. This work demonstrates the potential for injection locked VCSELs to be used in large-scale photonic quantum networks.

Funding. Department of Education, Skills and Employment, Australian Government (RTP);Australian Research Council (DE170100752).

Acknowledgements. The authors thank Keysight for the loan of a UXR1102A Infiniium UXR-Series oscilloscope.

Disclosures. The authors declare no conflicts of interest.

REFERENCES

1. J. Squier, Opt. Photon. News **13**, 42 (2002).
2. M. Akbulut, S. Bhooplapur, I. Ozdur, J. Davila-Rodriguez, and P. J. Delfyett, Opt. Express **18**, 18284 (2010).
3. H. J. Kimble, Nature **453**, 1023 (2008).
4. P. Kok, W. J. Munro, K. Nemoto, T. C. Ralph, J. P. Dowling, and G. J. Milburn, Rev. Mod. Phys. **79**, 135 (2007).
5. M. R. Sprague, P. S. Michelberger, T. F. M. Champion, D. G. England, J. Nunn, X.-M. Jin, W. S. Kolthammer, A. Abdolvand, P. S. J. Russell, and I. A. Walmsley, Nat. Photonics **8**, 287 (2014).
6. H. de Riedmatten, M. Afzelius, M. U. Staudt, C. Simon, and N. Gisin, Nature **456**, 773 (2008).
7. K. T. Kaczmarek, P. M. Ledingham, B. Brecht, S. E. Thomas, G. S. Thekkadath, O. Lazo-Arjona, J. H. Munns, E. Poem, A. Feizpour, D. J. Saunders, J. Nunn, and I. A. Walmsley, Phys. Rev. A **97**, 042316 (2018).
8. O. Katz and O. Firstenberg, Nat. Commun. **9**, 1 (2018).
9. N. Sangouard, C. Simon, H. de Riedmatten, and N. Gisin, Rev. Mod. Phys. **83**, 33 (2011).
10. J. Nunn, N. K. Langford, W. S. Kolthammer, T. F. M. Champion, M. R. Sprague, P. S. Michelberger, X. M. Jin, D. G. England, and I. A. Walmsley, Phys. Rev. Lett. **110**, 133601 (2013).
11. E. Knill, R. Laflamme, and G. J. Milburn, Nature **409**, 46 (2001).
12. M. Steiner, V. Leong, M. A. Seidler, A. Cerè, and C. Kurtsiefer, Opt. Express **25**, 6294 (2017).
13. J. J. Zayhowski and C. Dill, Opt. Lett. **19**, 1427 (1994).
14. T. L. Huang, S. C. Li, C. H. Tsou, H. C. Liang, K. F. Huang, and Y. F. Chen, Opt. Lett. **43**, 5753 (2018).
15. S. G. Rozuvan and E. A. Tikhonov, Quantum Electron. **25**, 337 (1995).
16. A. Larsson, E. Simpanen, J. S. Gustavsson, E. Haglund, E. P. Haglund, T. Lengyel, P. A. Andrekson, W. V. Sorin, S. Mathai, M. Tan, and S. R. Bickham, Opt. Fiber Technol. **44**, 36 (2018).
17. A. Dienes and L. W. Carr, J. Appl. Phys. **69**, 1766 (1991).
18. A. Gatto, A. Boletti, P. Boffi, and M. Martinelli, Opt. Express **17**, 21748 (2009).
19. B. Lane, B. Kose, J. M. Castro, and R. Pimpinella, J. Light. Technol. Vol. 30, Issue 15, pp. 2532-2541 **30**, 2532 (2012).
20. F. Mogensen, H. Olesen, and G. Jacobsen, IEEE J. Quantum Electron. **21**, 784 (1985).
21. V. A. Shchukin, N. N. Ledentsov, Z. Qureshi, J. D. Ingham, R. V. Penty, I. H. White, A. M. Nadtochy, M. V. Maximov, S. A. Blokhin, L. Y. Karachinsky, and I. I. Novikov, Appl. Phys. Lett. **104**, 051125 (2014).
22. R. Slavík and Z. Liu, J. Light. Technol. Vol. 38, Issue 1, pp. 43-59 **38**, 43 (2020).
23. T. Mori and H. Kawaguchi, Jpn. J. Appl. Physics, Part 2: Lett. **46**, L433 (2007).
24. C. Perrella, P. S. Light, J. D. Anstie, F. N. Baynes, F. Benabid, and A. N. Luiten, Opt. Lett. **38**, 2122 (2013).
25. C. Perrella, P. S. Light, S. A. Vahid, F. Benabid, and A. N. Luiten, Phys. Rev. Appl. **9**, 044001 (2018).
26. F. Nez, F. Biraben, R. Felder, and Y. Millerioux, Opt. Commun. **102**, 432 (1993).
27. A. V. Krishnamoorthy, K. W. Goossen, L. M. Chirovsky, R. G. Rozier, P. Chandramani, W. S. Hobson, S. P. Hui, J. Lopata, J. A. Walker, and L. A. D'asaro, IEEE Photonics Technol. Lett. **12**, 1073 (2000).

FULL REFERENCES

1. J. Squier, "Ultrafast optics," Opt. Photon. News **13**, 42–46 (2002).
2. M. Akbulut, S. Bhooplapur, I. Ozdur, J. Davila-Rodriguez, and P. J. Delfyett, "Dynamic line-by-line pulse shaping with GHz update rate," Opt. Express **18**, 18284 (2010).
3. H. J. Kimble, "The quantum internet," Nature **453**, 1023–1030 (2008).
4. P. Kok, W. J. Munro, K. Nemoto, T. C. Ralph, J. P. Dowling, and G. J. Milburn, "Linear optical quantum computing with photonic qubits," Rev. Mod. Phys. **79**, 135–174 (2007).
5. M. R. Sprague, P. S. Michelberger, T. F. M. Champion, D. G. England, J. Nunn, X.-M. Jin, W. S. Kolthammer, A. Abdolvand, P. S. J. Russell, and I. A. Walmsley, "Broadband single-photon-level memory in a hollow-core photonic crystal fibre," Nat. Photonics **8**, 287 (2014).
6. H. de Riedmatten, M. Afzelius, M. U. Staudt, C. Simon, and N. Gisin, "A solid-state light-matter interface at the single-photon level." Nature **456**, 773 (2008).
7. K. T. Kaczmarek, P. M. Ledingham, B. Brecht, S. E. Thomas, G. S. Thekkadath, O. Lazo-Arjona, J. H. Munns, E. Poem, A. Feizpour, D. J. Saunders, J. Nunn, and I. A. Walmsley, "High-speed noise-free optical quantum memory," Phys. Rev. A **97**, 042316 (2018).
8. O. Katz and O. Firstenberg, "Light storage for one second in room-temperature alkali vapor," Nat. Commun. **9**, 1–6 (2018).
9. N. Sangouard, C. Simon, H. de Riedmatten, and N. Gisin, "Quantum repeaters based on atomic ensembles and linear optics," Rev. Mod. Phys. **83**, 33 (2011).
10. J. Nunn, N. K. Langford, W. S. Kolthammer, T. F. M. Champion, M. R. Sprague, P. S. Michelberger, X. M. Jin, D. G. England, and I. A. Walmsley, "Enhancing multiphoton rates with quantum memories," Phys. Rev. Lett. **110**, 133601 (2013).
11. E. Knill, R. Laflamme, and G. J. Milburn, "A scheme for efficient quantum computation with linear optics," Nature **409**, 46–52 (2001).
12. M. Steiner, V. Leong, M. A. Seidler, A. Cerè, and C. Kurtsiefer, "Photon bandwidth dependence of light-matter interaction," Opt. Express **25**, 6294 (2017).
13. J. J. Zayhowski and C. Dill, "Diode-pumped passively Q-switched picosecond microchip lasers," Opt. Lett. **19**, 1427 (1994).
14. T. L. Huang, S. C. Li, C. H. Tsou, H. C. Liang, K. F. Huang, and Y. F. Chen, "Narrowing spectral linewidth in passively mode-locked solid-state lasers," Opt. Lett. **43**, 5753 (2018).
15. S. G. Rozuvan and E. A. Tikhonov, "Ultrashort pulse generation by synchronous pulsed pumping of a dye laser with a Sagnac-interferometer cavity," Quantum Electron. **25**, 337–340 (1995).
16. A. Larsson, E. Simpanen, J. S. Gustavsson, E. Haglund, E. P. Haglund, T. Lengyel, P. A. Andrekson, W. V. Sorin, S. Mathai, M. Tan, and S. R. Bickham, "1060 nm VCSELs for long-reach optical interconnects," Opt. Fiber Technol. **44**, 36–42 (2018).
17. A. Dienes and L. W. Carr, "Effect of the pulse shape on self-phase-modulation-induced chirping of optical pulses in diode laser amplifiers," J. Appl. Phys. **69**, 1766–1768 (1991).
18. A. Gatto, A. Boletti, P. Boffi, and M. Martinelli, "Adjustable-chirp VCSEL-to-VCSEL injection locking for 10-Gb/s transmission at 155 μm," Opt. Express **17**, 21748 (2009).
19. B. Lane, B. Kose, J. M. Castro, and R. Pimpinella, "Investigation of the Interaction of Modal and Chromatic Dispersion in VCSEL–MMF Channels," J. Light. Technol. Vol. 30, Issue 15, pp. 2532-2541 **30**, 2532–2541 (2012).
20. F. Mogensen, H. Olesen, and G. Jacobsen, "Locking conditions and stability properties for a semiconductor laser with external light injection," IEEE J. Quantum Electron. **21**, 784 (1985).
21. V. A. Shchukin, N. N. Ledentsov, Z. Qureshi, J. D. Ingham, R. V. Penty, I. H. White, A. M. Nadtochy, M. V. Maximov, S. A. Blokhin, L. Y. Karachinsky, and I. I. Novikov, "Digital data transmission using electro-optically modulated vertical-cavity surface-emitting laser with saturable absorber," Appl. Phys. Lett. **104**, 051125 (2014).
22. R. Slavík and Z. Liu, "Optical Injection Locking: From Principle to Applications," J. Light. Technol. Vol. 38, Issue 1, pp. 43-59 **38**, 43–59 (2020).
23. T. Mori and H. Kawaguchi, "Dynamical lasing wavelength variation in polarization bistable switching of vertical-cavity surface-emitting lasers by light injection," Jpn. J. Appl. Physics, Part 2: Lett. **46**, L433 (2007).
24. C. Perrella, P. S. Light, J. D. Anstie, F. N. Baynes, F. Benabid, and A. N. Luiten, "Two-color rubidium fiber frequency standard," Opt. Lett. **38**, 2122 (2013).
25. C. Perrella, P. S. Light, S. A. Vahid, F. Benabid, and A. N. Luiten, "Engineering Photon-Photon Interactions within Rubidium-Filled Waveguides," Phys. Rev. Appl. **9**, 044001 (2018).
26. F. Nez, F. Biraben, R. Felder, and Y. Millerioux, "Optical frequency determination of the hyperfine components of the two-photon transitions in rubidium," Opt. Commun. **102**, 432–438 (1993).
27. A. V. Krishnamoorthy, K. W. Goossen, L. M. Chirovsky, R. G. Rozier, P. Chandramani, W. S. Hobson, S. P. Hui, J. Lopata, J. A. Walker, and L. A. D'asaro, "16 × 16 VCSEL array flip-chip bonded to CMOS VLSI circuit," IEEE Photonics Technol. Lett. **12**, 1073–1075 (2000).